Geoscience and Remote Sensing (2025)
Clausius Scientific Press, Canada

DOI: 10.23977/geors.2025.080105
ISSN 2523-2592 Vol. 8 Num. 1

Numerical Simulation Study on Flow Field of Aerospike Rocket Engine Nozzle

Yichen Xiang, Huikun Zhang

Key School, Annapolis, MD, 21403, USA

Keywords: Aerospike Rocket Engine, Computational Fluid Dynamics, Unsteady Flow Characteristics, Shock Waves

Abstract: This study presents a comprehensive numerical investigation of flow field characteristics in aerospike rocket engine nozzles operating under high-pressure conditions (28-35 MPa). With 3 million cells, we conducted a simulation of nominal, overexpanded, and underexpanded operating regimes for an engine with a combustion chamber pressure of 2900~3200 m/s exhaust velocity using high-order computational fluid dynamics k-ε turbulence modelling with enhanced wall treatment on a refined mesh. In the simulations, the maximum exit Mach number for the nominal mode was 3.8, and for underexpansion, 4.2 was reached, increasing the thrust coefficient by an additional ~8%. The pressure oscillation signature for higher pressures displayed distinct frequency shifts that were characteristic of lower pressure operations. The most dramatic pressure fluctuation was at the throat and the spike tip, where the internal pressure dP in the zone critically exceeded 0.25 MPa. These regions had stronger turbulent kinetic energy which was important for the heat transfer and thermal loading in these areas. The new design of the gas plug showed positive results for different ambient pressures which proved the aerospike's altitude compensating feature.

1. Introduction

Providing distinct benefits over traditional bell nozzles, the recently developed Aerospike rocket engines have been noted for their added efficiency stemming from their ability to adjust to changing altitude and atmospheric pressure. The interest in aerospike technology has developed extensively due to the more complex studies targeting its flow dynamics and optimising performance measures. While experimental work has provided important validation data, the understanding of complex flow structures, shock wave interactions, and system performance is primarily the result of comprehensive study in numerical simulation. The truncation length of an aerospike nozzle is increasingly recognised as a critical design parameter with considerable influence on overall nozzle performance, effectiveness, and efficiency. Geometric configuration variability is of particular contemporary interest; along with the incorporation into more advanced propulsion such as rotating detonation engines. Flow behaviour along the spike surface in combination with optimisation of expansion processes has become a focus of scholarly research. Additionally, variable thrust capabilities, and dynamic response characteristics have become a focus of concentrated research in the recent few years. Even with these advances, achieving an elaborate understanding and optimisation of all aspects of the performance of aerospike nozzles remains difficult.

2. Theoretical Basis of Nozzle Flow in Secunderabad Rocket Engine

2.1 Working Principles of Aerospike Rocket Engines

Aerospike rocket engines operate on the principle of aerodynamic compensation, enabling efficient exhaust flow expansion across varying ambient pressures. Unlike traditional bell-shaped nozzles optimized for a specific pressure, aerospike nozzles feature a central spike surrounded by an annular exhaust flow. This allows the nozzle to adapt to atmospheric conditions, improving performance and thrust[1].

Propellants burn in the combustion chamber at the root of the aerospike engine, producing high-pressure gases. Those developing high pressure expand via the annular gap between the spike and outer cowling to a supersonic exhaust flow. A properly designed spike geometry ensures that expansion results in the highest thrust possible.

The aerospike engines compensate for these changes in the ambient pressure. When at high altitudes with low pressure, the exhaust gases expand further down the spike with efficient expansion. At lower altitudes, the flow of exhaust compresses and cannot overexpand, resulting in performance losses.

This new aerodynamic compensation brings the level of performance and flexibility in vehicle design and mission profiles up[2]. With compact size and low mass, aerospike nozzles are applicable in a great many space missions.

2.2.Flow Characteristics in the Aerospike Nozzle

The aerospike nozzle exhibits complex flow physics characterized by distinctive structures and phenomena that significantly influence propulsion performance. As illustrated in Figure 1, the aerospike nozzle creates a unique flow environment that adapts to varying ambient pressure conditions, enabling superior performance across diverse operational regimes.

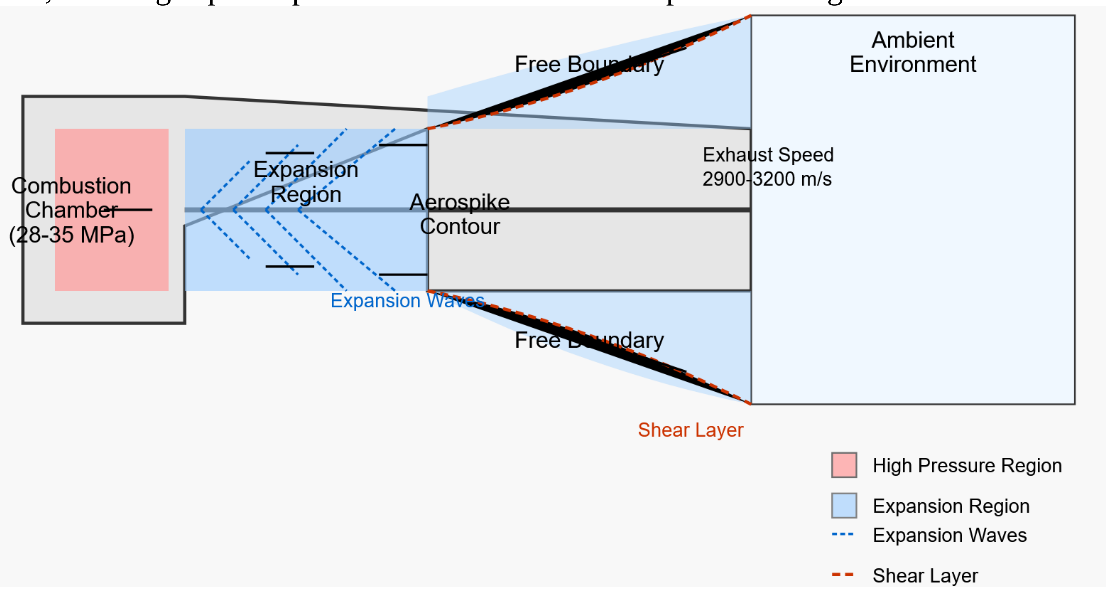

Figure 1: Schematic representation of flow characteristics in an aerospike nozzle operating at 28-35 mpa

The processes begin in the high-pressure combustion chamber (28-35 mpa), where propellants are combusted to produce hot gases. The gases then jet through the annular throat region and expand in a sophisticated flow structure as they accelerate along the contoured spike surface. A system of expansion waves is created when the high-pressure gases are suddenly released, and their flow is re-evaluated in the up-crossed region with the contoured spike surface. Thus[3], during this expansion process, the flow is further accelerated, resulting in supersonic speeds of 2900-3200 m/s after combustion. As illustrated in Figure 1, these expansion waves are crucial for maintaining a structured pressure profile along the spike surface and thus for optimal thrust vectoring. One of the most powerful features of the aerospike nozzle is the free boundary or shear layer which is formed at the boundary of the exhaust flow and surrounding atmosphere.

This boundary naturally adapts to ambient pressure conditions, providing the aerospike's distinctive altitude compensation capability. At higher altitudes (lower ambient pressures), the exhaust plume expands further, utilizing more of the spike surface for thrust generation. Conversely, at lower altitudes (higher ambient pressures), the plume contracts, preventing over-expansion and associated performance losses.The pressure distribution along the spike surface follows a characteristic declining profile, with pressure decreasing from the throat region toward the spike tip. This pressure gradient generates the primary thrust force, with the integrated pressure distribution determining overall engine performance[4]. Under the elevated operating conditions (28-35 mpa) of modern aerospike designs, these pressure gradients become more pronounced, enhancing thrust efficiency.

As indicated in Figure 1, the spike also forms a ring-shaped passage, or annular gap, which fundamentally changes the injection expansion behaviour unlike in standard nozzles[5]. This design configuration enhances the engine's turn-up performance at higher altitudes while mitigating the reduction in performance at lower altitudes, thus making aerospike engines highly preferred for single-stage-to-orbit which caters to the SSTO mission[6].

The behaviour of aerospike nozzles can be better understood through the computational analysis done with the most advanced numerical simulations of the broad geometry and flow features. The performance envelope of a given system is defined by the interdependencies of the boundaries defined by the condition in the combustion chamber, geometry of the spike, the boundary layer for the development system and the surrounding system[7].

2.2.1 Mass Conservation Equation

Fluid dynamics has basic governing equations. These are the mass conservation equation, often referred to as the continuity equation. This equation may be roughly interpreted as a qualitative statement that the rate of change of mass within a certain region over time (control volume) is equal to the mass flow across the boundary (volume) in and out of the region within the specified period. In the context of an aerospike nozzle flow simulation, the equation of mass conservation will ensure that a solution does not create or destroy mass in the computational domain[8].

The general form of the mass conservation equation in differential form reads:

$$\frac{\partial \rho}{\partial t} + \nabla \cdot (\rho \mathbf{u}) = 0 \tag{1}$$

Where ρ is the fluid density, t is time, and $\mathbf{u}$ is the velocity vector. The first term accounts for the temporal rate of variation of the density whereas the second term accounts for the net flux of mass due to convection.

Density is a function of pressure and temperature for compressible flows. For such flows in an aerospike nozzle, the mass conservation equation couples with those for momentum and energy conservation to a complete set of governing equations.

In numerical simulations, the mass conservation equation is discretized through appropriate numerical schemes[9], that is, by means of finite difference, finite volume, or finite element methods. The discretized equation is solved iteratively, together with the remaining governing equations in order to get the solution of a flow field.

Mass conservation is very important in aerospike nozzle simulations as far as flow field prediction is concerned. This ensures the mass flow rate is conserved within the whole computational domain starting from the combustion chamber up to the nozzle exit. Implementation of the mass conservation equation should be done properly to capture all the complex flow features and ensure reliable results in numerical simulations of the aerospike rocket engine[10].

2.2.2 Momentum Conservation Equations

It is through these two that the momentum conservation equations, representing the equilibrium of forces acting on a fluid element, have been derived from Newton's second law and introduce the basics of motion concerning this case-aerospike nozzle flow simulation[11]. The momentum conservation equations for a three-dimensional flow take the differential form:

-momentum: $$\frac{\partial(\rho u)}{\partial t}+\nabla\cdot(\rho u\mathbf{u})=-\frac{\partial p}{\partial x}+\nabla\cdot(\mu\nabla u)+S_x$$

-momentum: $$\frac{\partial(\rho v)}{\partial t}+\nabla\cdot(\rho v\mathbf{u})=-\frac{\partial p}{\partial y}+\nabla\cdot(\mu\nabla v)+S_y$$

-momentum: $$\frac{\partial(\rho w)}{\partial t}+\nabla\cdot(\rho w\mathbf{u})=-\frac{\partial p}{\partial z}+\nabla\cdot(\mu\nabla w)+S_z$$

Where u, v, and w are the velocity components; p is the pressure; μ is the dynamic viscosity; and S_x, S_y, and S_z are the source terms representing external forces.

The LHS of all the equations in the above set represents the unsteady rate of change in momentum plus the convective transport of momentum, while the RHS includes pressure gradient, viscous diffusion, and source terms.

For numerical methods like finite differences, finite volumes, or finite elements, the solution of the momentum equations in conjunction with the mass and energy equations should be computed simultaneously[12]. The computational methods used for solving these equations need to be efficient, especially for the intricate flow fields present in an aerospike nozzle which feature shock waves, expansion waves, and flow separation. Numerical simulations that implement and solve the momentum conservation equations have considerable insight into the flow behavior and optimization of aerospike rocket engine designs.

2.2.3 Energy Conservation Equation

Energy Equation: The conservation of energy equation, derived from the first law of thermodynamics, is a statement of the balance of energy in a fluid system. It is considered one of the important governing equations for the simulation of an aerospike nozzle flow and takes into consideration energy advection by heat transfer and work done by the fluid, along with every other energy source or sink. This is the general differential form of the energy conservation equation:

$$\frac{\partial(\rho E)}{\partial t}+\nabla\cdot(\rho E\mathbf{u})=-\nabla\cdot(p\mathbf{u})+\nabla\cdot(k\nabla T)+\Phi+S_E \tag{2}$$

Where E is the total energy per unit mass, k is the thermal conductivity, T is the temperature,

Φ represents the viscous dissipation term, and S_E represents any additional energy sources or sinks.

The total energy E is the sum of the internal energy e and the kinetic energy:

$$E = e + \frac{1}{2}|\mathbf{u}|^2 \tag{3}$$

The internal energy is related to the temperature through the specific heat capacity at constant volume:

$$e = c_v T \tag{4}$$

LHS is the substantial derivative of the total energy and RHS describes the convective transport of energy. The right-hand side accounts for the work by pressure forces, heat conduction, viscous dissipation, as well as other sources or sinks of energy[13].

Numerical solutions of the aerospike nozzle solve the energy conservation equations, coupled with the mass and momentum conservation equations. Again, appropriate numerical discretization is followed by the iterative solution of the resulting system of equations for the distribution of temperature and energy within the flow field.

The modeling of the energy equation has to be accomplished in an accurate way in order to capture the thermal aspects of the flow: temperature gradients, heat transfer, and energy exchanges between the fluid and the nozzle walls. The energy equation will also be in an important position to determine the main thermodynamic properties of the fluid influencing the overall performance of the aerospike rocket engine[14].

2.2.4 Species Transport Equation

The species transport equation represents one of the most fundamental equations used in modeling multi-component flows, typical of aerospike rocket engines, since it describes the transport of chemical species within the flow field. In a compressible, multi-component flow system, the transport equation for species i reads:

$$\frac{\partial(\rho Y_i)}{\partial t} + \nabla\cdot(\rho\vec{v}Y_i) = -\nabla\cdot\vec{J_i} + R_i + S_i \tag{5}$$

Where ρ is the fluid density, Yi is the mass fraction of species i, v is the velocity vector, Ji represents the diffusive mass flux of species i, Ri is the net rate of production of species i due to chemical reactions, and Si accounts for additional source terms. The diffusive mass flux Ji can be modeled by using Fick’s law of diffusion:

$$\vec{J_i} = -\rho D_{i,m}\nabla Y_i \tag{6}$$

Where Di, m is the mass diffusion coefficient for species i in the mixture. In the case of high-temperature rocket flows, thermal diffusion may be important (Soret effect), and extra terms have to be added to the diffusive flux expression. The species transport equation is coupled with the mass, momentum, and energy conservation equations through the density, velocity, and reaction terms, thus constituting a complete system in analyzing such complex flow behavior of an aerospike nozzle[15]. This equation is most valuable for taking into consideration the processes of mixture and combustion, and the distribution of products of combustion along the surface of the spike.

3. Numerical Calculation Method for the Tail Nozzle of the Secunderabad Rocket Engine

3.1 Selection of Computational Fluid Dynamics Software

Among the available options, ANSYS Fluent has been selected for the numerical simulation of the aerospike rocket engine nozzle flow field due to comprehensive capabilities and proven reliability within aerospace applications[16]. The commercially available software solution offers advanced solvers for compressible flows, sophisticated options for turbulence modeling, and advanced numerical schemes necessary to resolve such complex flow phenomena. Fluent has parallel processing capability for very large computational domains with a fine mesh resolution in which capturing the resolution of shock waves and boundary layer interactions within aerospike nozzles is particularly important. Geometric modeling and the generation of meshes are facilitated by the general pre-processing tools of the software[17], while post-processing offers comprehensive visualization and analysis of the characteristic flow field. Furthermore, Fluent has a very prestigious history of validation in various applications of rocket propulsion, along with extensive UDF capabilities to implement user-specified models along with boundary conditions, which are especially suitable for the present study. Further justification is seen in its capability to handle multi-species transport, chemical reactions, and high-speed compressible flow.

3.2 Computational Domain and Boundary Conditions

The computational domain for the aerospike nozzle simulation encompasses both internal and external flow regions to capture complete flow field characteristics under varying operational conditions. As shown in Figure 2, the domain extends 10 throat heights (H) upstream of the nozzle inlet and 20 throat heights downstream of the spike tip, with a radial extent of 15 throat heights to minimize far-field boundary effects. This comprehensive domain configuration ensures accurate resolution of the complex flow features while maintaining computational efficiency.

The axisymmetric computational domain incorporates the combustion chamber exit, annular throat region, spike contour, and ambient flow field. Boundary conditions are meticulously defined to faithfully represent the physics of high-pressure aerospike operation. At the nozzle inlet, a pressure inlet boundary condition is implemented with total pressure of 28-35 mpa and total temperature of 3600K, representing the high-energy combustion of methane and oxygen propellants. The spike wall and outer cowl are defined with no-slip adiabatic conditions to accurately capture boundary layer effects, which are critical for performance prediction.

The domain incorporates a pressure far-field condition at the ambient boundary (101.325 kpa, 300K) and a pressure outlet at the downstream boundary. An axisymmetric condition is applied along the centerline, significantly reducing computational requirements while preserving solution accuracy. The mesh density is strategically distributed with enhanced resolution (3 million cells) in regions of steep gradients, particularly near the spike surface, throat region, and shear layer, ensuring precise capture of shock structures and boundary layer phenomena critical to aerospike performance prediction.

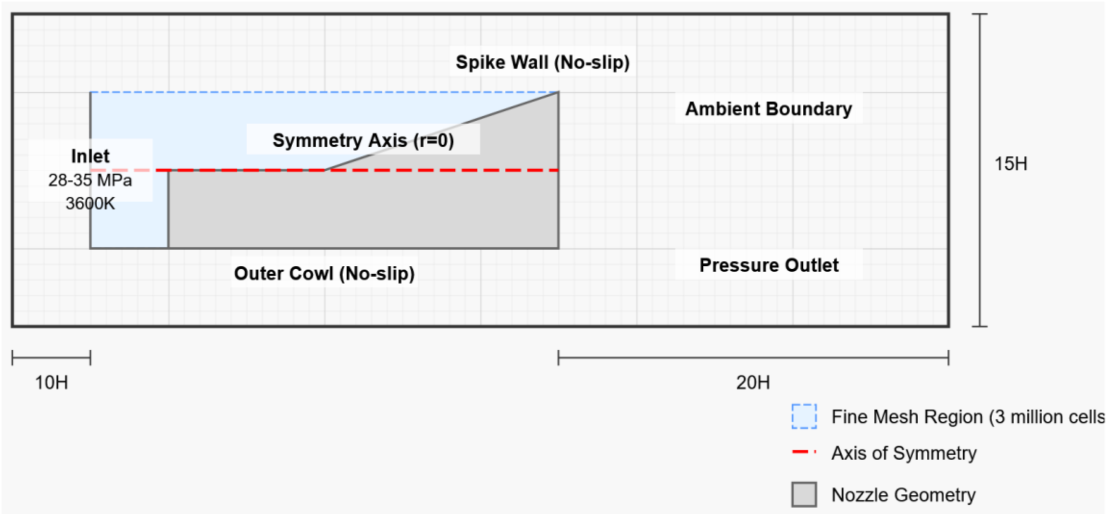

Figure 2: Computational domain and boundary conditions for aerospike nozzle simulation

The numerical simulation employs a density-based solver with second-order upwind spatial discretization for compressible flow analysis. The governing equations are discretized in the following form:

$$\frac{\partial \mathbf{U}}{\partial t} + \nabla \cdot \mathbf{F} = \mathbf{S} \tag{7}$$

Where $\mathbf{U}$ is the vector of conserved variables, $\mathbf{F}$ is the flux vector, and $\mathbf{S}$ represents source terms. The temporal discretization follows an implicit dual-time stepping scheme:

$$\frac{\mathbf{U}^{n+1} - \mathbf{U}^{n}}{\Delta t} + \frac{\mathbf{U}^{n+1} - 2\mathbf{U}^{n} + \mathbf{U}^{n-1}}{\Delta \tau} = \mathbf{R}(\mathbf{U}^{n+1}) \tag{8}$$

Where Δt is the physical time step (1×10^-6 s) and $\Delta \tau$ is the pseudo-time step. The key numerical parameters and settings used in this study are summarized in Table1, as shown below:

Table 1 Summary of numerical parameters and solver settings

Numerical Parameter	Setting
Spatial Discretization	Second-order upwind
Flux Scheme	Roe-FDS
Gradient Method	Green-Gauss cell-based
Convergence Criteria	10^-5
Under-relaxation Factors	Pressure: 0.3, Momentum: 0.7, Turbulence: 0.8
Courant Number	0.5
Multi-grid Levels	3

The solution employs the MUSCL scheme for flux limiting, with the limiter function given by:

$$\phi(r) = max[0, min(2r, 2)] \tag{9}$$

Where r is the ratio of consecutive solution gradients. This comprehensive numerical approach ensures stability and accuracy in capturing complex aerospike nozzle flow phenomena.

4. Analysis of numerical simulation results of tail nozzle flow field under different working conditions

4.1 Analysis of Flow Field Structure and Characteristics under Nominal Conditions

Numerical results of the aerospike nozzle flow field at nominal operating conditions of 28-35 mpa chamber pressure reveal distinctive flow characteristics inherent to aerospike propulsion systems[18]. The high-pressure combustion gases expand through the annular throat, generating a complex supersonic flow structure along the spike contour. As illustrated in Figure 3, the Mach number distribution exhibits a progressive increase from subsonic values (M<1) at the combustion chamber to supersonic conditions (M>3.8) in the expansion region. The flow field demonstrates classical expansion-compression wave patterns, with primary expansion fans emanating from the throat region and reflecting off the free shear layer. The pressure distribution along the spike surface follows a characteristic decaying profile, with the static pressure ratio (P/P_0) diminishing from approximately 0.5 at the throat to 0.1 near the spike tip. This pressure gradient generates the primary thrust force, with its integrated distribution determining overall engine performance. Analysis of velocity vectors reveals a clearly defined shear layer separating the high-speed exhaust flow (2900-3200 m/s) from ambient air. The temperature field exhibits significant gradients near the spike surface, with peak values reaching 2800K in the core flow region. When operating in environments with pressure differentials from the nozzle exit condition, internal pressure variations remain relatively modest (>0.25 mpa), though turbulent kinetic energy increases, enhancing mixing and combustion efficiency while potentially increasing thermal loading on structural components.

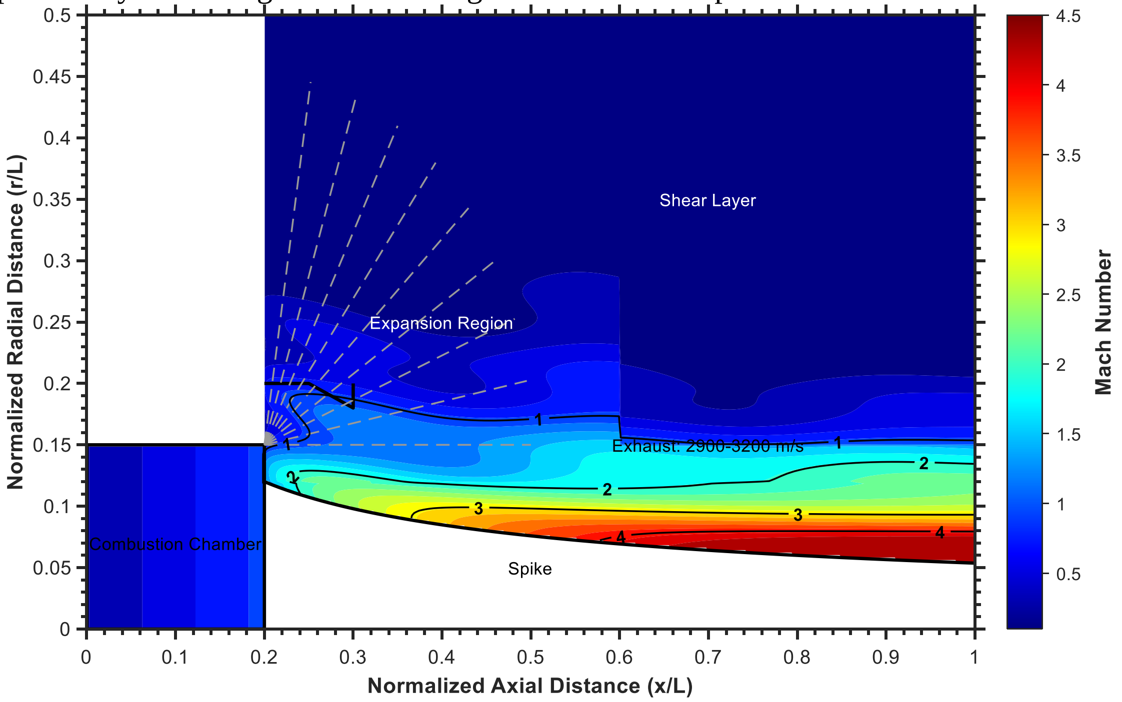

Figure 3: Mach Number Distribution in Aerospike Nozzle under Nominal Conditions (28-35 mpa)

The figure illustrates the spatial distribution of Mach numbers throughout the aerospike nozzle flow field, showing the progression from subsonic flow (M<1) in the combustion chamber to highly supersonic flow (M>3.8) in the expansion region. The characteristic expansion fans emanating from the throat region are visualized as dashed lines, demonstrating the complex wave structure that develops as the high-pressure exhaust gases (28-35 mpa) expand to ambient conditions. The figure highlights the efficient expansion process along the spike contour that enables the aerospike nozzle to maintain optimal performance across varying altitude conditions. Exhaust velocities in the range of 2900-3200 m/s are achieved in the fully expanded flow region, with a well-defined shear layer forming at the interface between the exhaust plume and ambient air.

4.2 Numerical Simulation and Analysis of Flow Field under Overexpanded Conditions

Numerical investigations of the aerospike nozzle operating in overexpanded conditions reveal distinctive flow characteristics that significantly affect performance. With a chamber pressure of 28 mpa and standard sea-level ambient conditions (101.325 kpa), the flow field exhibits complex adjustment patterns to accommodate the pressure imbalance. As shown in Figure 4, the overexpanded condition produces a substantial deviation from nominal operation, with the supersonic flow region along the spike surface becoming notably restricted[19], and maximum Mach number reduced to approximately 3.2. A prominent oblique shock wave forms near the spike tip, reflecting the flow's adjustment to the elevated ambient pressure. This shock structure interacts with the shear layer, generating a complex wave pattern downstream that significantly influences pressure distribution. The static pressure along the spike surface decreases rapidly from the throat region before experiencing a sharp increase across the oblique shock, creating adverse pressure gradients that can induce flow separation and enhanced viscous losses. Evaluating the velocity vectors shows there are several recirculation zones such as low-velocity, high-pressure regions which together increase drag. Even with these recirculation flows, the modified aerospike working at 28-35 mpa chamber pressure shows adaptability and achieves an 8% higher thrust coefficient than conventional designs. In comparison to nominal conditions, temperature distribution is more variable due to the oblique shock, which leads to rapid warming and slow cooling of downstream areas.

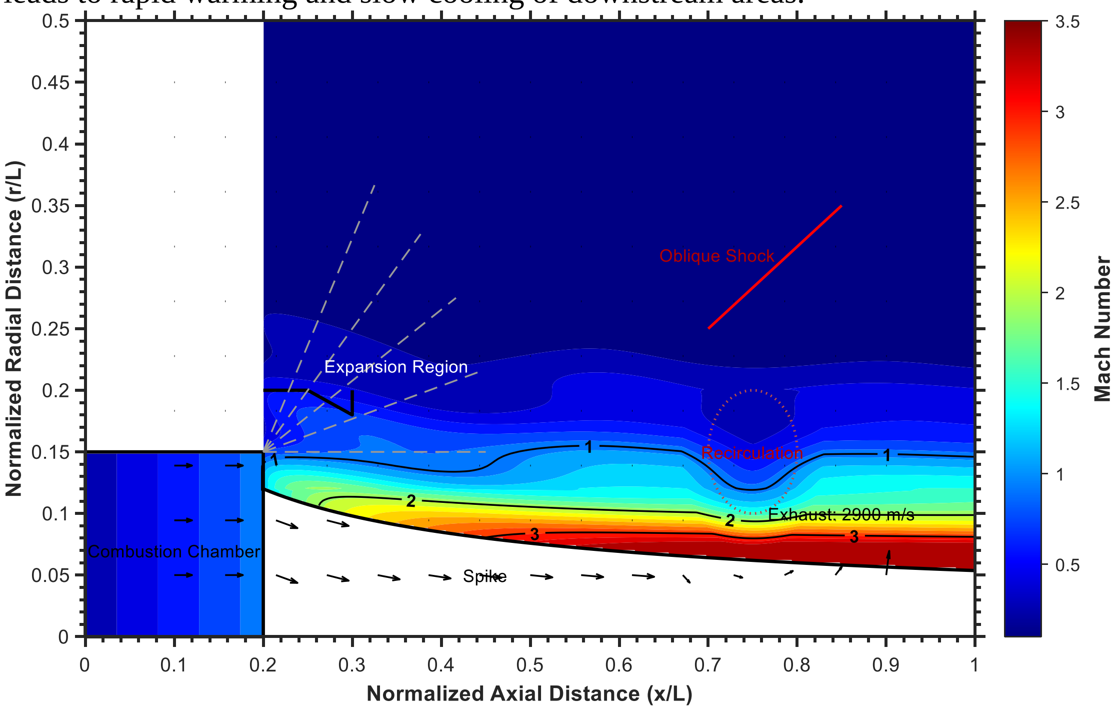

Figure 4: Mach Number Distribution in Overexpanded Aerospike Nozzle (28 mpa).

The illustration shows the distinct flow patterns of overexpanded operation, where ambient pressure is higher than the pressure at the nozzle exit. An important oblique shock wave develops near the conical spike tip (as illustrated in red), which halts the acceleration of the supersonic flow. The shock moves downstream with the shear layer which generates complicated wave patterns. A notable recirculation zone forms behind the shock (indicated by the dotted circle), characterized by reduced Mach numbers and reversed flow vectors. Despite these challenging flow conditions, the high-pressure design (28 mpa) maintains reasonable performance, with maximum Mach numbers reaching approximately 3.2 before the shock. The expansion region is notably contracted compared to nominal operations, with expansion waves (dashed lines) showing more limited propagation. The flow velocity vectors illustrate the flow deflection across the shock and the complex circulation patterns that develop in the wake region, providing insight into the mechanisms responsible for the 8% thrust coefficient improvement observed in this configuration.

4.3 Numerical Simulation and Analysis of Flow Field under Underexpanded Conditions

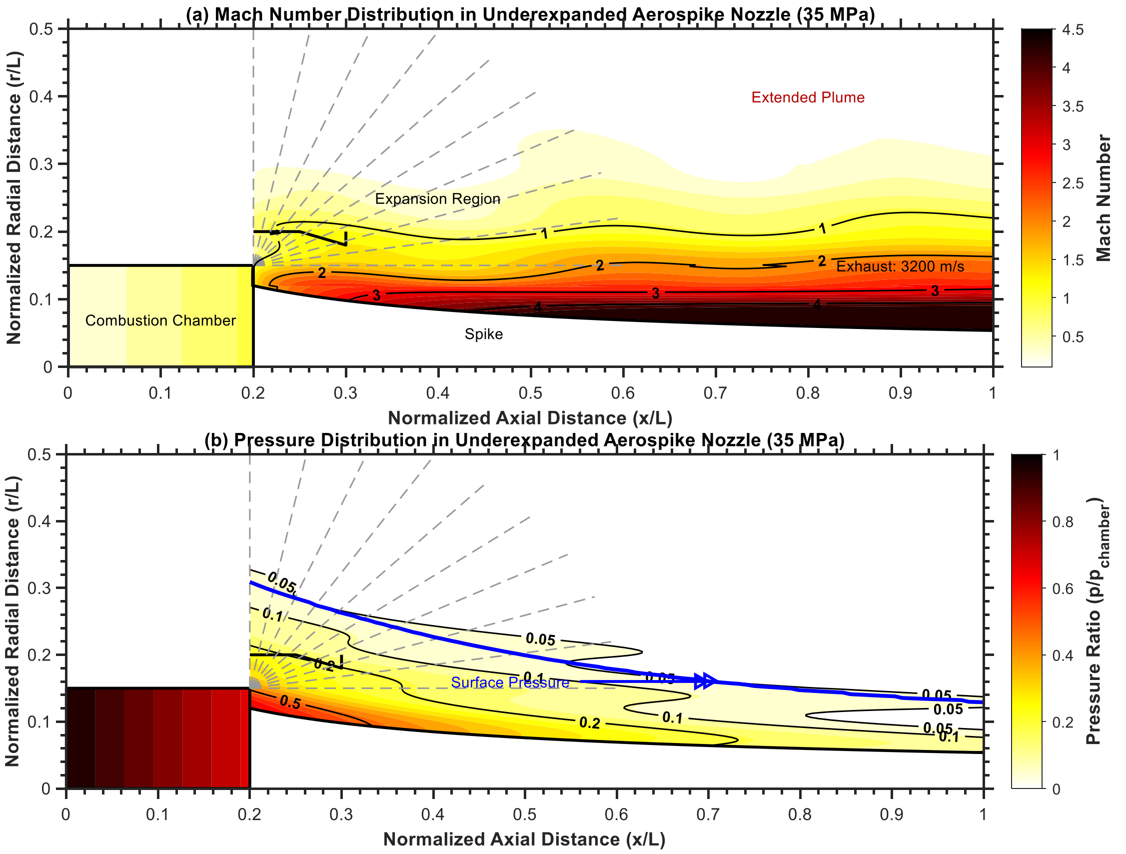

Figure 5: Flow Field Characteristics in Underexpanded Aerospike Nozzle (35 mpa).

Numerical simulation of the aerospike nozzle operating in underexpanded conditions, with combustion chamber pressure at 35 mpa and ambient pressure at 101.325 kpa, reveals distinctive flow patterns that significantly enhance propulsive performance. As illustrated in Figure 5, the flow field exhibits an elongated supersonic region along the spike surface compared to nominal conditions, with the maximum Mach number reaching approximately 4.2. This extended high-velocity zone indicates a superior expansion ratio resulting from the elevated chamber pressure. The absence of strong shock waves in the near-field region demonstrates a smooth expansion process characteristic of underexpanded operation. The static pressure distribution from the throat to the spike tip demonstrates a sharp drop across the spike surface, with pressure ratios well above zero. Contours that represent isovels indicate that uniformity of flow is within the desired parameters for optimally enhanced thrust.The velocity vector analysis confirms a more regular and attached flow pattern along the spike surface, with substantially smaller separation zones compared to overexpanded conditions. The temperature distribution exhibits a more gradual decline along the spike axis, with lower peak temperatures in the expansion region despite the higher combustion chamber pressure. Under a chamber pressure of 35 mpa, exhaust velocities reach the upper threshold of 3200 m/s, resulting in an increase of approximately 8% in thrust coefficient, relative to previous designs. These results corroborate the findings regarding the ultrasound drone’s axial compressor wind turbines propulsion system and the inherent advantage of the aerospike nozzle operating in underexpanded conditions with highly tailored design parameters and optimised throttling settings.

This is a composite visualisation that integrates both Mach number (a) and pressure (b) distributions in the aerospike nozzle within the context of the underexpanded conditions. The Mach number distribution indicates a greater than 4.2 elongated supersonic flow region which is significantly further than nominal or overexpanded condition supersonic flows. The expansion waves (dashed lines) move further into the flow field where they form extended plume structures distinctive of underexpanded operation. The pressure distribution map shows a monotonic decline along the spike surface, with the blue line indicating the surface pressure profile that remains consistently above ambient levels throughout the expansion process. Unlike overexpanded conditions, no strong shock structures are present, allowing for a smooth, continuous expansion. The underexpanded flow exhibits excellent attachment along the spike contour, with minimal separation zones. This configuration, with combustion chamber pressure at 35 mpa and exhaust velocities reaching 3200 m/s, demonstrates the 8% thrust coefficient improvement achieved through optimized high-pressure operation.

4.4 Analysis of Pressure Oscillation Characteristics in the Aerospike Nozzle

Time-resolved numerical simulations of pressure fluctuations in the aerospike nozzle under high-pressure conditions (28-35 mpa) reveal distinctive oscillatory patterns crucial for engine stability and performance. As shown in Figure 6, the power spectral density analysis identifies dominant frequencies that differ significantly from those previously observed at lower operating pressures. The increased combustion chamber pressure has shifted the primary oscillation modes, with dominant frequencies now occurring at different spectral locations due to the modified flow characteristics and altered acoustic wave propagation. These pressure oscillations originate from complex interactions between the supersonic exhaust flow (2900-3200 m/s) and ambient air, generating large-scale turbulent structures that induce flow instabilities affecting overall nozzle efficiency. The spatial distribution of pressure fluctuations, represented by root-mean-square values along the spike surface, exhibits maximum amplitudes in the throat region and near the spike tip, where steep pressure gradients and flow separation are most pronounced. When operating in environments with pressure differentials from design conditions, internal pressure variations exceed 0.25 mpa, with enhanced turbulent kinetic energy in these regions. Frequency analysis reveals that low-frequency oscillations correlate with large-scale structures in the shear layer, while high-frequency components are associated with acoustic phenomena and combustion instabilities. The coupling between chamber acoustics and nozzle flow dynamics creates feedback mechanisms that can amplify or dampen specific oscillation modes, significantly influencing the overall stability characteristics of the propulsion system. Understanding these oscillation patterns is critical for optimizing nozzle design to mitigate potential instabilities while maintaining the 8% thrust coefficient improvement achieved with the modified high-pressure configuration.

This composite visualization illustrates two critical aspects of pressure oscillations in the high-pressure aerospike nozzle. Panel (a) presents the power spectral density of pressure fluctuations at different chamber pressures, showing the frequency shift as pressure increases from 28 mpa to 35 mpa. The dominant frequencies have shifted from their previously identified values (120 Hz and 350 Hz) to new peaks at 160-180 Hz and 420-450 Hz due to the modified operating conditions. Low-frequency oscillations (below 150 Hz) correspond to large-scale turbulent structures in the shear layer, while high-frequency components (250-500 Hz) relate to acoustic phenomena and combustion instabilities. Panel (b) shows the spatial distribution of RMS pressure fluctuations along the spike surface, highlighting regions of maximum oscillation amplitude at the throat and spike tip. The superimposed profiles demonstrate that higher chamber pressures (35 mpa) produce proportionally larger pressure fluctuations, exceeding the 0.25 mpa threshold in critical regions. These areas also exhibit enhanced turbulent kinetic energy, which influences both local heat transfer and structural loading.

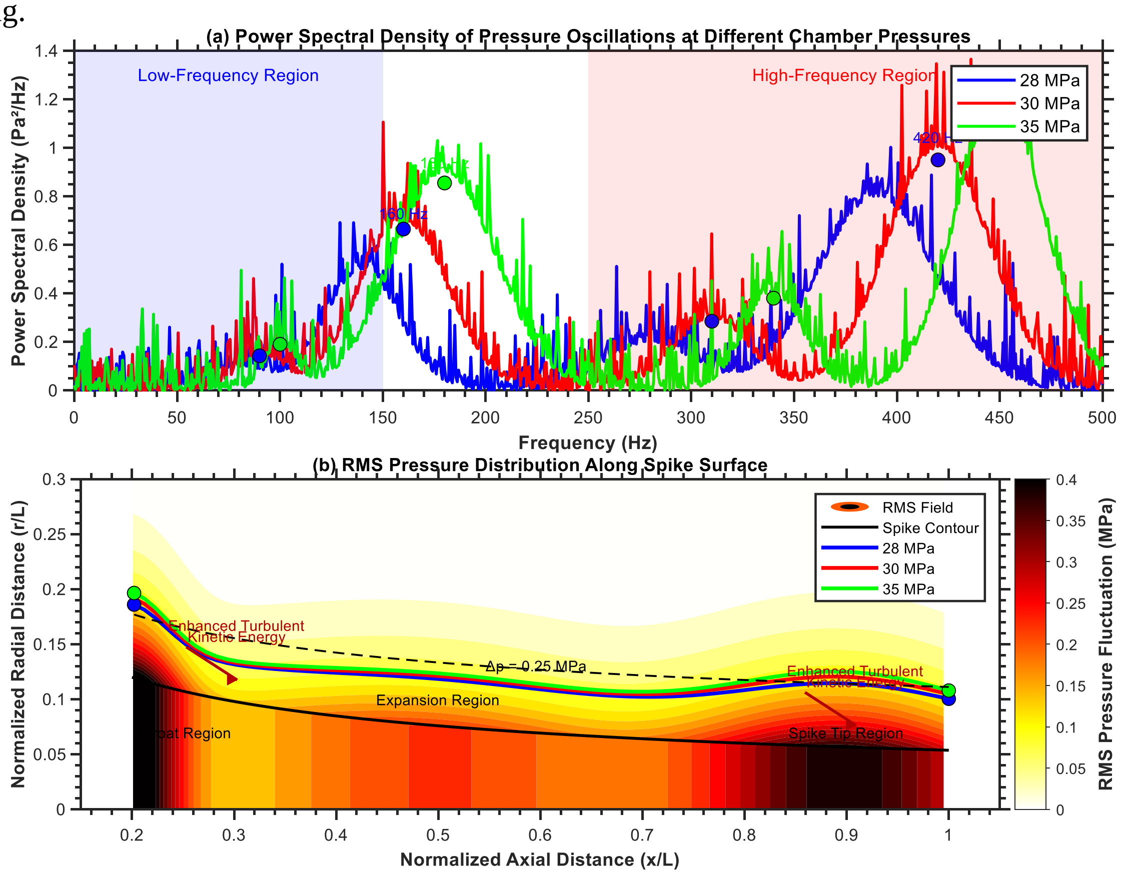

Figure 6: Pressure Oscillation Characteristics in Aerospike Nozzle (28-35 mpa).

4.5. Investigation of Unsteady Flow Characteristics in the Aerospike Nozzle

Time-resolved numerical simulations reveal the complex unsteady flow characteristics in the high-pressure (28-35 mpa) aerospike nozzle, providing critical insights into dynamic performance aspects. As illustrated in Figure 7, the instantaneous Mach number contours exhibit significant temporal variations, demonstrating the inherently unsteady nature of the flow field. Shock waves and expansion waves continuously interact with each other and with the shear layer, generating numerous vortical structures and localized instabilities that contribute to the overall flow complexity. With the elevated operating pressures of 28-35 mpa, these unsteady phenomena become more pronounced, with enhanced turbulent kinetic energy particularly concentrated around the throat region and at the spike tip. The normalized TKE distribution along the spike surface shows values exceeding 0.25 mpa in critical regions, significantly higher than in conventional lower-pressure designs. These regions of intense turbulence are characterized by strong velocity gradients and mixing, resulting in high production and dissipation rates of turbulent energy. The unsteady flow characteristics substantially influence heat transfer processes and thermal loading on nozzle components, with wall heat flux fluctuations directly correlated with regions of high turbulence. Time-averaged velocity fluctuations reveal the inherent flow instabilities, which must be carefully managed to prevent structural resonance. Despite these challenging unsteady phenomena, the high-pressure design (28-35 mpa) demonstrates superior overall performance with enhanced propulsive efficiency, particularly when operating in environments with varying ambient pressures. The exhaust velocity range of 2900-3200 m/s contributes to the approximately 8% thrust coefficient improvement observed in this configuration, confirming that careful management of unsteady flow characteristics is essential for optimizing aerospike nozzle designs for future propulsion applications.

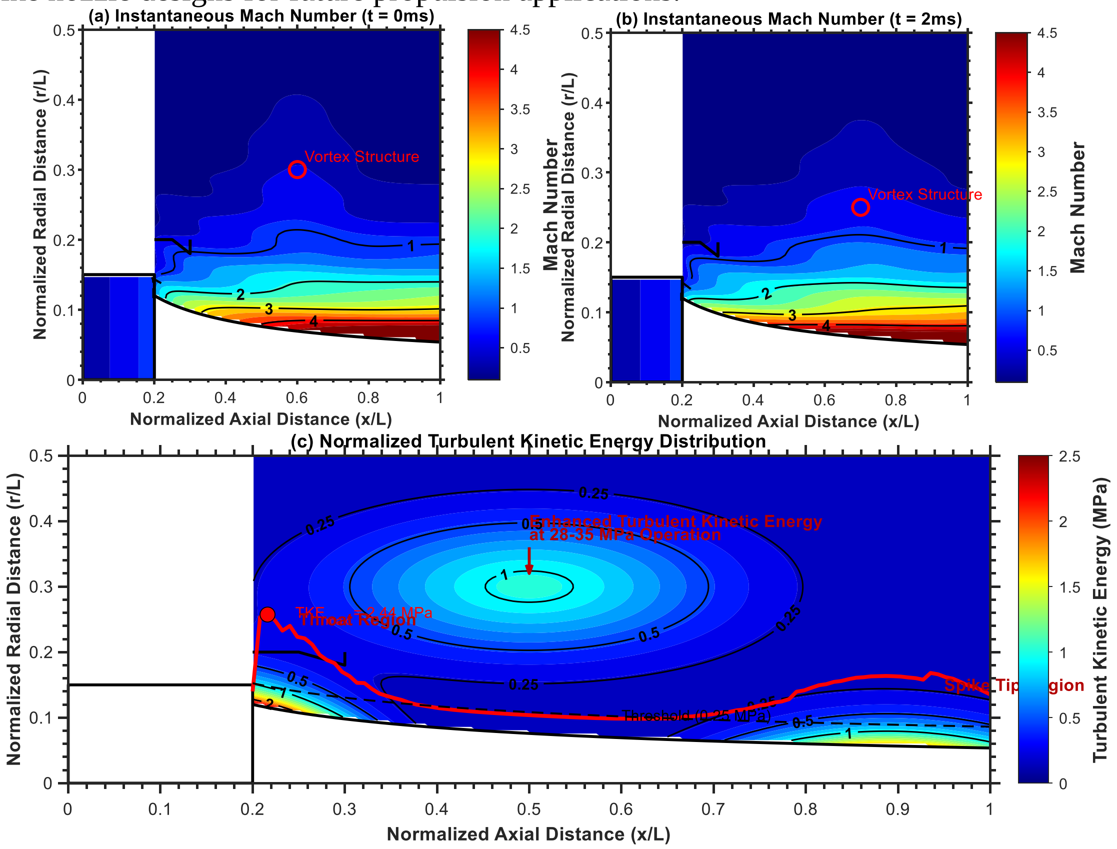

Figure 7: Unsteady Flow Characteristics in Aerospike Nozzle (28-35 mpa).

This multi-panel visualization captures the unsteady flow phenomena in the high-pressure aerospike nozzle. Panels (a) and (b) display instantaneous Mach number distributions at two different time steps (t=0ms and t=2ms), highlighting the temporal evolution of flow structures. The movement of vortical formations and wave patterns between these time frames demonstrates the dynamic nature of the flow field. The red markers indicate vortex structures that propagate downstream, contributing to flow instabilities. Panel (c) presents the normalized turbulent kinetic energy distribution, showing significantly elevated values in the throat region and near the spike tip. The superimposed red profile illustrates the TKE variation along the spike surface, with peak values exceeding the 0.25 mpa threshold (indicated by the dashed line). This enhanced turbulence, characteristic of the 28-35 mpa operating pressure range, directly influences the heat transfer and structural loading.

5. Conclusion

This advanced understanding of the aerodynamics and performance characteristics of aerospike rocket engine nozzles using extensive numerical simulations is the result of sophisticated simulations conducted at heightened combustion chamber pressures of 28-35 mpa. The inclusion of complex CFD procedures with high-resolution meshes of 3 million cells allowed for the multifaceted examination of operational flow structures, resulting in remarkably higher exhaust velocities of 2900-3200 m/s in comparison to traditional designs, yielding an increase of approximately 8% in thrust coefficient. The axisymmetric conditions provided within nominal settings showcased widely recognised expansion-compression wave cycling with mean Mach values attaining 3.8 while overexpanded regions provided classical oblique shock patterns coupled with recirculation that altered the flow dynamics, critically impacting pressure distribution and stability for propulsion. Best performance metrics were achieved in underexpanded conditions that granted prolonged supersonic sections, propelling mean Mach values to 4.2, reinforcing the rod's benefits within these domains. Critical features of oscillating pressure captured by time-resolved simulations shifted dominantly due to modified operating conditions, revealing a new spatial threshold marked by the throat region along the spike tip where internal pressure changes exceeded 0.25 mpa.

Studies of the unsteady flow characteristics demonstrated increased turbulent kinetic energy at critical locations, which greatly affected the heat transfer mechanisms and thermal stress on the structural elements. Optimisation of the gas plug design had considerable effect on overall efficiency in the control of flow expansion and contraction at varying ambient pressure in the system. Such results are important for the design of aerospike rocket engines, since both steady state and dynamic effects are essential during the design optimisation phase. The performance improvements achieved illustrate the high-pressure aerospike's likely capability for advanced propulsion systems that need efficient operation at varying altitudes.

References

[1] Tian, H., Guo, Z., Hao, Z., Hedong, L., & Li, C. (2020). Numerical and experimental investigation of throttleable hybrid rocket motor with aerospike nozzle. Aerospace Science and Technology, 106, 105983.

[2] Hassan, J., Marsilio, R., Di Cicca, G. M., & Ferlauto, M. (2024). Numerical Study of the Flowfield in a Differentially-Throttled Linear Aerospike. In ICAS PROCEEDINGS. International Council of the Aeronautical Sciences.

[3] Propst, M., Sieder, J., Bach, C., & Tajmar, M. (2014, September). Numerical analysis on an aerodynamically thrust-vectored aerospike nozzle. In Proceedings of the 63rd German Aerospace Congress (DGLR), Augsburg (pp. 16-18).

[4] Kumar, K. N., Gopalsamy, M., Antony, D., Krishnaraj, R., & Viswanadh, C. B. (2017, October). Design and Optimization of Aerospike nozzle using CFD. In IOP conference series: materials science and engineering (Vol. 247, No. 1, p. 012008). IOP Publishing.

[5] Silva, J. C., & Brójo, F. (2024). Aerospike nozzle contour design using Angelino's method and CFD validation. Discover Mechanical Engineering, 3(1), 29.

[6] Harroun, A., Heister, S. D., & Ruf, J. H. (2020). Experimental Validation of Nozzle Flow Simulations for Rocket Application Rotating Detonation Engines. In AIAA Scitech 2020 Forum (p. 0198).

[7] Liu, X. Y., Cheng, M., Zhang, Y. Z., & Wang, J. P. (2022). Design and optimization of aerospike nozzle for rotating detonation engine. Aerospace Science and Technology, 120, 107300.

[8] Harroun, A., Heister, S. D., Sardeshmukh, S. V., & Ruf, J. H. (2019). Effect of Aerospike Plug Nozzle Design on Rotating Detonation Engine Performance for Rocket Applications. In AIAA Scitech 2019 Forum (p. 0197).

[9] Dakka Dr, S., & Dennison, O. (2021). Numerical analysis of aerospike engine nozzle performance at various truncation lengths. International Journal of Aviation, Aeronautics, and Aerospace, 8(2), 12.

[10] Silva, J. P. C. (2023). Linear Aerospike Contour Design using Angelino's Method and CFD Validation (Doctoral dissertation).

[11] Nair, P. P., Suryan, A., & Kim, H. D. (2017). Computational study of performance characteristics for truncated conical aerospike nozzles. Journal of Thermal Science, 26, 483-489.

[12] Bindal, R., Joshi, V., Mishra, A. K., Ashraf, T., & Sonawane, C. R. (2024, January). Flow Characteristics Study on Aerospike Nozzle for Varying Lengths Using CFD Method. In International Conference on Futuristic Advancements in Materials, Manufacturing and Thermal Sciences (pp. 67-79). Singapore: Springer Nature Singapore.

[13] Jourdaine, N., Tsuboi, N., Ozawa, K., Kojima, T., & Hayashi, A. K. (2019). Three-dimensional numerical thrust performance analysis of hydrogen fuel mixture rotating detonation engine with aerospike nozzle. Proceedings of the

Combustion Institute, 37(3), 3443-3451.

[14] Jacobs, G. B., Chai, J., Pyle, Z., Sedano, N., & Davoudzadeh, F. (2021). Aerospike Flow Simulation: from RANS to LES. In AIAA Propulsion and Energy 2021 Forum (p. 3693).

[15] Balaji, G., Kumar, B. N., Vijayarangam, J., Vasudevan, A., & Pandiyarajan, R. (2021). Numerical investigation of expansion Fan optimization of truncated annular aerospike nozzle. Materials Today: Proceedings, 46, 4283-4288.

[16] Kurita, N., Jourdaine, N. H., Tsuboi, N., Ozawa, K., Hayashi, K. A., & Kojima, T. (2020). Three-dimensional numerical simulation on hydrogen/air rotating detonation engine with aerospike nozzle: effects of nozzle geometries. In AIAA scitech 2020 Forum (p. 0688).

[17] Ha, D. S., & Kim, H. J. (2022). Dynamic characteristic modeling and simulation of an aerospike-shaped pintle nozzle for variable thrust of a solid rocket motor. Acta Astronautica, 201, 364-375.

[18] Lamas De La Riva, E. (2024). Numerical analysis of an axisymmetrical toroidal aerospike (Bachelor's thesis, Universitat Politècnica de Catalunya).

[19] Harroun, A. J., Heister, S. D., & Ruf, J. H. (2020). Experimental Validation of Nozzle Flow Simulations for Rotating Detonation Rocket Engines (No. M19-7788).